

Real Space Imaging of Spin Polarons in Zn Doped SrCu₂(BO₃)₂

M. Yoshida,¹ H. Kobayashi,¹ I. Yamauchi,¹ M. Takigawa,¹ S. Capponi,²
D. Poilblanc,² F. Mila,³ K. Kudo,⁴ Y. Koike,⁵ and N. Kobayashi⁶

¹*Institute for Solid State Physics, University of Tokyo, Kashiwa, Chiba 277-8581, Japan*

²*Laboratoire de Physique Théorique, Université de Toulouse and CNRS, UPS (IRSAMC), F-31062 Toulouse, France*

³*Institut de Théorie des Phénomènes Physiques, École Polytechnique Fédérale de Lausanne, CH-1015 Lausanne, Switzerland*

⁴*Department of Physics, Okayama University, Okayama 700-8530, Japan*

⁵*Department of Applied Physics, Tohoku University, Sendai 980-8579, Japan*

⁶*Institute for Materials Research, Tohoku University, Sendai 980-8577, Japan*

(Dated: September 5, 2018)

We report on the real space profile of spin polarons in the quasi two-dimensional frustrated dimer spin system SrCu₂(BO₃)₂ doped with 0.16% of Zn. The ¹¹B nuclear magnetic resonance spectrum exhibits 15 additional boron sites near non-magnetic Zn impurities. With the help of exact diagonalizations of finite clusters, we have deduced from the boron spectrum the distribution of local magnetizations at the Cu sites with fine spatial resolution, providing direct evidence for an extended spin polaron. The results are confronted with those of other experiments performed on doped and undoped samples of SrCu₂(BO₃)₂.

PACS numbers: 75.25.-j, 76.60.Pc, 75.10.Jm

Impurities and defects in strongly correlated quantum systems often produce significant effects over an extended spatial region, which can be studied by local probes such as nuclear or electron magnetic resonance (NMR or ESR) [1]. The best example is the edge states in Heisenberg spin chains. The spin 1/2 edge state in spin 1 Haldane chains is a direct consequence of the valence-bond-solid ground state of the pure system. The ESR experiments have played vital roles in identifying the edge spins [2, 3] and their interactions [4]. The edge states are not localized at a single site but associated with local staggered magnetization due to the antiferromagnetic interaction of the bulk, and the spatial extent of such a polaronic structure is given by the correlation length of the bulk. The real space profile of spin polarons has been actually observed by NMR experiments in both spin 1 [5, 6] and spin 1/2 [7] Heisenberg chains, from which the temperature dependence of the correlation length was deduced.

Although there have been less studies on two-dimensional (2D) systems, an interesting example is the frustrated 2D dimer spin system SrCu₂(BO₃)₂ with a small concentration of Cu²⁺ ions (spin 1/2) replaced by non-magnetic Zn or Mg [8–11]. The magnetic layers contain orthogonal arrays of Cu dimers described by the Shastry-Sutherland lattice [12]

$$H = J \sum_{n,n.} \mathbf{S}_i \cdot \mathbf{S}_j + J' \sum_{n,n.n.} \mathbf{S}_i \cdot \mathbf{S}_j, \quad (1)$$

where J (J') is the intradimer (interdimer) Heisenberg exchange interaction. The ground state of SrCu₂(BO₃)₂ at zero magnetic field is the dimer singlet state [13, 14], which is known to be the exact ground state of Eq. (1) for $\alpha = J'/J$ not too large [12, 15], less than $\alpha_c \simeq 0.675$ [16, 17]. SrCu₂(BO₃)₂ exhibits a number of fascinating properties, most notably a unique sequence of quantized

magnetization plateaus in magnetic fields [18–23] which have been a subject of intense research in the last decade [24, 25].

A nonmagnetic impurity creates an unpaired Cu²⁺ site in the dimer singlet state, producing a free spin-1/2. The structure factor of this spin-1/2 measured by inelastic neutron scattering experiments [10] points to an extended object. Theories have confirmed this picture and moreover predicted the formation of a spin polaron extending over several sites around the impurity [9, 11], clearly calling for further precise experimental information.

In this letter, we report the observation of such a spin polaron in real space by ¹¹B NMR experiments on Zn doped SrCu₂(BO₃)₂ performed in a sufficiently high magnetic field to saturate unpaired spins. With the help of exact diagonalization results, a nearly complete assignment of the 15 additional boron sites has been achieved, leading to the determination of the microscopic structure of a localized spin polaron with unprecedented accuracy.

Single crystals of SrCu_{2-x}Zn_x(BO₃)₂ were grown by the traveling-solvent floating-zone method [26, 27]. Two crystals were used, $x = 0.0174$ and 0.0032 as determined by the inductively coupled plasma atomic emission spectrometry. The presence of free spins at low temperatures was confirmed by magnetization measurements (see Supplementary Material (Suppl. Mat.) A [28]). The crystals were cut into a rod ($1 \times 1 \times 5$ mm³) for NMR measurements, which were performed in a magnetic field B of 6.615 T precisely along the c axis (within ~ 0.2 degree).

The NMR spectra were obtained by summing the Fourier transform of the spin-echo signal obtained at equally spaced rf-frequencies. Figure 1 shows the ¹¹B NMR spectrum for $x = 0.0032$ (0.16% of Zn) at 1.6 K. The Zeeman energy for the magnetic field of 6.615 T is much smaller than the zero-field energy gap for the triplet

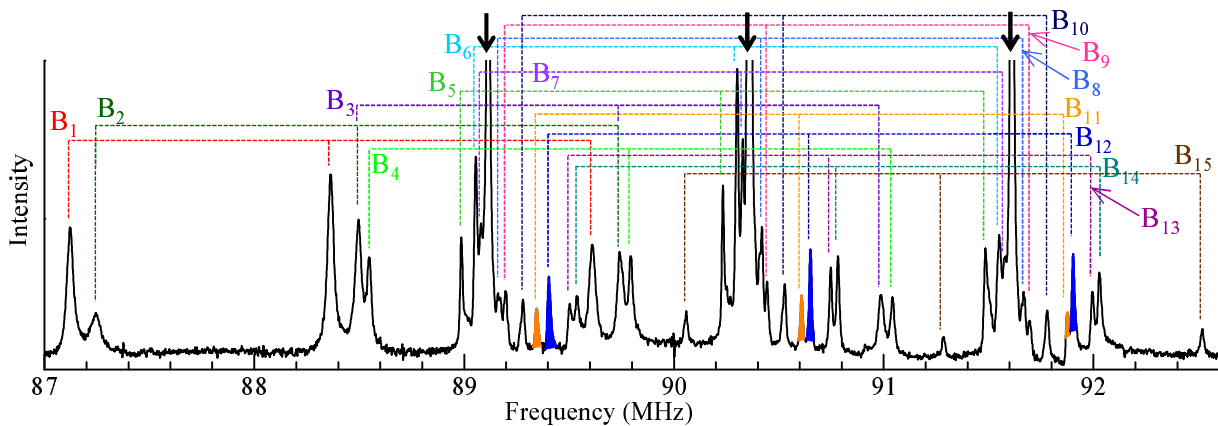


FIG. 1: (color online) ^{11}B NMR spectrum at $T = 1.6$ K and $B = 6.615$ T. The black arrows mark the position of the reference line (zero internal field). 15 additional lines named B_1 to B_{15} have been resolved. Note that B_1 is about twice as intense as B_2 , and that B_{12} (shaded in blue) is also about twice as intense as B_{11} (shaded in orange).

excitation in the bulk ($\Delta = 35$ K) but large enough to completely polarize the impurity induced free spins (see Suppl. Mat. A and B [28]). To understand the ^{11}B NMR spectra, we first recall that one boron site generates three NMR lines at the frequencies $\nu_r = \gamma(B + B_{\text{int}}) + k\nu_Q$, ($k = -1, 0, 1$), where ν_Q is the quadrupole splitting along the c axis, $\gamma = 13.66$ MHz/T is the nuclear gyromagnetic ratio, and B_{int} is the internal magnetic field produced by nearby Cu spins. Since the Zn concentration is extremely dilute, most of Cu spins form singlet dimers generating $B_{\text{int}} \sim 0$ at the majority of B sites. The NMR lines from these B sites (shown by black arrows) are very intense, far exceeding the range of display in Fig. 1.

In addition to this reference line, we have been able to identify 15 weaker lines with non-zero B_{int} ($B_1 - B_{15}$, the thin lines in Fig. 1) and to determine the values of B_{int} and ν_Q for each of them. The sample with $x = 0.0174$ gives a nearly identical NMR spectrum (see Suppl. Mat. C [28]), ensuring no interference between impurities.

As we shall demonstrate, it is possible to assign most of the lines to specific boron sites, and to deduce the polarization of the Cu sites around the impurity as shown in Fig. 2. To perform this line assignment, it is useful to know *a priori* the local magnetization expected in the neighborhood of a Zn impurity. We have thus performed exact diagonalizations (ED) calculation for finite-size clusters of the 2D Shastry-Sutherland lattice with 32 sites (31 spins and one vacancy) and 36 sites (35 spins and one vacancy), with periodic boundary conditions (see Suppl. Mat. D [28]). The ED results of Fig. 3(c) show that the local magnetization is distributed primarily over five spins surrounding the defect. A single spin at Cu_A with a large positive $\langle S_c^A \rangle \sim 0.18 - 0.30$, two spins at Cu_C with also a large positive $\langle S_c^C \rangle \sim 0.18 - 0.21$, and two spins at Cu_B with a large negative $\langle S_c^B \rangle \sim -0.1$ add up approximately to the saturated value of 0.5. In addition, eight spins at four other sites (Cu_{D-G}) carry a

small and oscillating magnetization less than 0.1 in absolute value. The local magnetization is much smaller for the remaining sites ($\sim 10^{-3}$) and cannot be determined accurately for the cluster sizes of our calculation. Interestingly, there is a strong dependence on α . First of all, the polaronic structure collapses very rapidly when α exceeds 0.68, where the pure system undergoes a first-order transition from the dimer to the plaquette phase [16, 17, 32]. Besides, and more remarkably, the magnetization of the unpaired site Cu_A , $\langle S_c^A \rangle$, strongly depends on α . It decreases steeply with α and becomes smaller than $\langle S_c^C \rangle$ at $\alpha \sim 0.66$, an observation that will turn crucial for the analysis of the experimental spectrum.

To make contact between the local magnetization at Cu sites and the boron spectrum, we note that the internal field B_{int} at a given boron site is given by the sum of contributions from neighboring Cu sites

$$B_{\text{int}}^i = \sum_j A_{ij} \langle S_c^j \rangle. \quad (2)$$

Here A_{ij} is the hyperfine coupling constant from the i -th boron site to the j -th Cu site. It is the sum of the dipolar and transferred hyperfine couplings, $A_{ij} = D_{ij} + T_{ij}$, and depends on the relative position between the boron and Cu sites. The dominant couplings are illustrated in Fig. 3(a) and summarized in Table I. The transferred hyperfine couplings are short-ranged and limited to the nearest and next-nearest neighbors in the same layer, T_1 and T_2 . They satisfy the condition $T_1 + 2T_2 = -0.431$ T imposed by the NMR shift data in undoped $\text{SrCu}_2(\text{BO}_3)_2$ [14], leaving only one adjustable parameter, say T_1 . The analysis of NMR spectra in the magnetization plateau phases has led to the estimation $-0.71 < T_1 < -0.53$ T [22]. The dipolar couplings can be calculated from the crystal parameters. In addition to the nearest and next-nearest neighbors in the same layer, two neighbors on the adjacent layers have significant dipolar couplings with

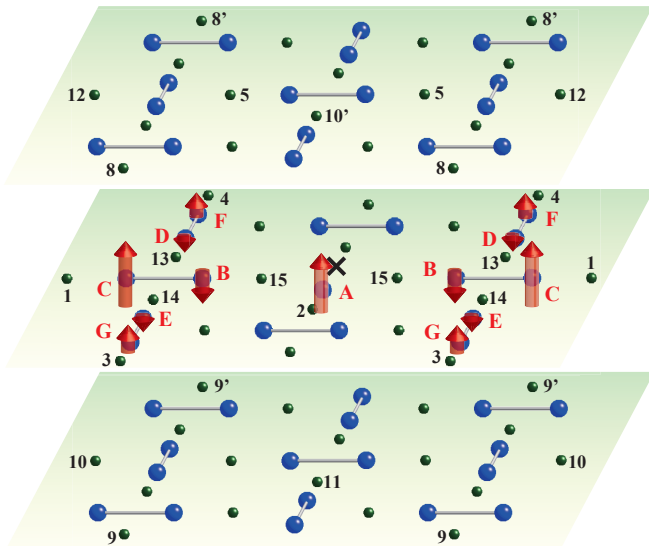


FIG. 2: (color online) Real space sketch of the spin polaron formed around a Zn impurity (cross). The up (down) arrows on the Cu sites represent the spin moments parallel (antiparallel) to the external field. The length of the arrow is proportional to $|\langle S_z \rangle|$ as calculated on a 36-site cluster with $J'/J = 0.67$. The numbers show the assignment of the B sites to the NMR lines of Fig. 1 deduced from the analysis described in the text. Primed numbers have been used when different sites are assigned to the same line. The other B sites have very small internal field.

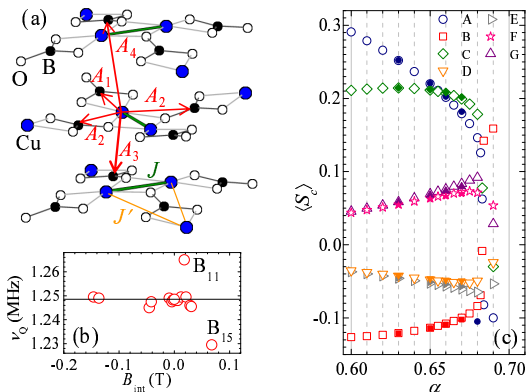


FIG. 3: (color online) (a) Main hyperfine couplings between a Cu spin and the B nuclei in the same layer (A_1 and A_2) or in the neighboring layers (A_3 or A_4). (b) Quadrupolar splitting ν_Q for B sites near a Zn impurity. (c) Dependence on $\alpha = J'/J$ of the local magnetization calculated with exact diagonalizations on a 32-site cluster (open symbols) and 36-site cluster (solid symbols).

different values $D_3 > D_4$ because of the buckling of the layers. Looking at Table I, we can anticipate that the boron sites close to the impurity both in the layer of the impurity and in the two adjacent layers will have internal fields large enough to give rise to additional peaks.

The absolute value of A_j is by far the largest for the

TABLE I: Hyperfine coupling constants in Tesla.

j	T_j	D_j	A_j
1	$-0.711 \sim -0.531$	-0.161	$-0.872 \sim -0.692$
2	$0.05 \sim 0.14$	-0.075	$-0.025 \sim 0.065$
3	0	0.103	0.103
4	0	0.065	0.065

nearest neighbor ($j = 1$). The value of B_{int} for the B sites in the layer of the impurity should, therefore, be primarily determined by $\langle S_c \rangle$ of the nearest neighbor Cu site. We then conclude that B_1 and B_2 , which show large negative B_{int} (~ -0.14 T, see Fig. 1), must correspond to the boron sites next to either Cu_A or Cu_C in Fig. 2. Likewise, B_{15} , with its large positive B_{int} (~ 0.07 T), should be next to Cu_B . The values of $\langle S_c^A \rangle$ and $\langle S_c^C \rangle$ can be estimated approximately as $B_{\text{int}}/A_1 \sim 0.2$, which is significantly smaller than the saturated value of 0.5. Thus the distribution of B_{int} provides a direct experimental proof for the polaronic spin structure near defects.

Interestingly, the integrated intensity of the low frequency satellite line of B_1 at 87.12 MHz is twice as large as that of B_2 at 87.24 MHz. Since each Zn impurity creates one Cu_A and two Cu_C sites, B_1 (B_2) must be assigned to boron sites next to Cu_C (Cu_A). The larger value of $|B_{\text{int}}|$ at B_1 then leads us to conclude that $\langle S_c^A \rangle < \langle S_c^C \rangle$. Fig. 3(c) shows that this condition is met only in a very narrow range of α between 0.655 and 0.68.

Thanks to this assignment, we are now in a position to fix α and T_1 by fitting the experimental value of B_{int} at the B_1 and B_2 sites using the 36-site cluster results (interpolated between $\alpha = 0.66$ and 0.67). This leads to $\alpha = 0.665$ and $T_1 = -0.563$ T ($A_1 = -0.724$, $A_2 = -0.009$ T), compatible with the values in Table 1. The full theoretical histogram of B_{int} deduced from Eq. (2) is plotted in the upper panels of Fig. 4(a) and (b). The isolated red lines in Fig. 4(a) represent B_{int} at the boron sites in the same layer as the impurity. Each of them is nearest to one of the seven Cu sites (Cu_A – G) carrying appreciable magnetization. The overall agreement between the ED results and experiment is very good, leading to the assignment of the lines B_3 , B_4 , B_{13} , B_{14} , and B_{15} (see Fig. 2).

Since other boron sites in the layer of the impurity have much smaller internal fields, we now turn to the neighboring layers. They have smaller values of B_{int} coming from the interlayer dipolar couplings D_3 or D_4 as shown in the upper panel of Fig. 4(b). Again, the agreement with the experimental results is very good. Let us focus on the experimental lines B_{11} and B_{12} . Since B_{12} is twice as intense as B_{11} (see Fig. 1), we must assign B_{12} to the neighbors of Cu_C in the layer above, and B_{11} to the neighbor of the Cu_A in the layer below. Since both couplings are given by D_3 , the larger B_{int} at B_{12} than B_{11} provides

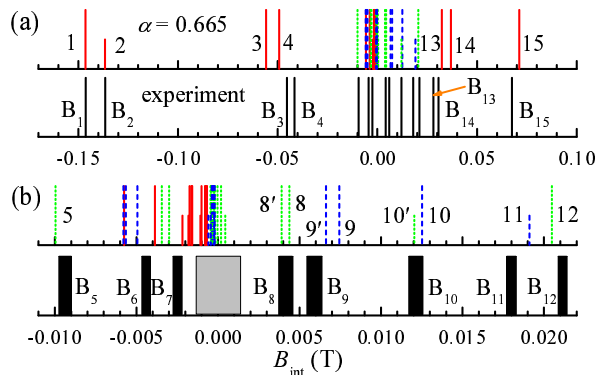


FIG. 4: (color online) (a) B_{int} at the B sites calculated by using the spin density distribution with $\alpha = 0.665$ for 36 sites (upper panel) and B_{int} deduced from experiment (lower panel). The data near $B_{\text{int}} = 0$ T are expanded in Fig. 4(b). The thickness of the lines in the lower panel indicates the half width at the half maximum of the corresponding peaks of the NMR spectrum. In the calculated histograms, red solid lines correspond to B sites in the layer of the Zn impurity, green dotted (blue dashed) lines to B in the adjacent layer above (below) the impurity, and the height is proportional to the number of B sites having exactly the same internal field (1 or 2).

an independent confirmation that $\langle S_c^A \rangle < \langle S_c^C \rangle$. With its strongly negative B_{int} , the line B_5 must be attributed to the neighbors of Cu_B in the layer above. Discussion on the other lines is given in the Suppl. Mat. E [28].

So far we have assumed that the hyperfine couplings are not influenced by Zn-doping. However, the small difference in the ionic radii between Cu^{2+} and Zn^{2+} (about 5% [33]) could produce non-uniform chemical pressure effects, which may result into a local lattice distortion and a modification of the hyperfine couplings. To estimate such effects, the quadrupole splitting ν_Q is a useful probe since it is sensitive to changes in local structure and charge density. The inset (b) of Fig. 3 shows the values of ν_Q for all the observed B NMR lines. Remarkably, most sites have exactly the same value $\nu_Q = 1.25$ MHz as in undoped $\text{SrCu}_2(\text{BO}_3)_2$ (solid line). Only the lines B_{11} and B_{15} show minor deviations of about 0.02 MHz, indicating that the effects of lattice distortion are small and limited to the immediate vicinity of the Zn impurities. Note that ν_Q at the boron sites close to Cu_A and Cu_C is unchanged, an indication that the hyperfine couplings are likely to remain the same. Furthermore, the dipolar coupling, which varies slowly with distance as $1/r^3$, should not be affected by a small lattice distortion. Therefore, our conclusion $\langle S_c^A \rangle < \langle S_c^C \rangle$ should remain valid even allowing for a local distortion around the impurity.

Finally, let us compare the values of α reported so far from various measurements. The analysis of susceptibility and specific heat data of the undoped material by the Shastry-Sutherland model with an inter-layer coupling has led to the best value $\alpha = 0.635$ [24],

while the recent determination of the width of the $1/2$ plateau in very high magnetic fields up to 118 T [23] led to $\alpha \simeq 0.63$. These values are smaller than our estimate $\alpha = 0.665$ necessary to account for the internal structure of the polaron. After discarding other possibilities such as Dzyaloshinsky-Moriya (we checked with ED for the Zn doped system that neither the intradimer nor the interdimer Dzyaloshinsky-Moriya coupling was able to account for the discrepancy), we came to the conclusion that the most likely explanation is that the ratio α increases near Zn due to the local chemical pressure induced by the larger ionic radius of Zn^{2+} as compared to Cu^{2+} . Indeed, a similar effect has already been observed in undoped samples under hydrostatic pressure [34]. To actually demonstrate that this local modification could explain the discrepancy, we have examined a simple model in which the Cu-Cu bond closest to Zn, i.e. the Cu_A - Cu_B bond J_{imp} is allowed to change from the bulk J' (see Suppl. Mat. F [28]). We found that the polaronic structure derived from NMR is actually compatible with $\alpha \simeq 0.65$ if J_{imp} is allowed to take larger values in the range $0.72 - 0.77$. This value of α is already significantly lower than the estimate 0.665 for the uniform system, and it sounds plausible that this value can be further lowered if one allows for additional modifications of the coupling constants. It would be interesting to investigate this possibility further with the help of ab-initio investigations of the local exchange couplings of Zn doped. This however goes far beyond the scope of the present paper.

We acknowledge useful discussions with C. Berthier and M. Horvatić. The work was supported by Grant-in-Aids for JSPS KAKENHI (B) (No. 21340093), the MEXT-GCOE program, and the Swiss National Foundation. Numerical simulations were performed at CALMIP and GENCI.

-
- [1] H. Alloul, J. Bobroff, M. Gabay, and P. J. Hirschfeld, Rev. Mod. Phys. **81**, 45 (2009).
 - [2] M. Hagiwara, K. Katsumata, I. Affleck, B. I. Halperin, and J. P. Renard, Phys. Rev. Lett. **65**, 3181 (1990).
 - [3] S. H. Glarum, S. Geschwind, K. M. Lee, M. L. Kaplan, and J. Michel, Phys. Rev. Lett. **67**, 1614 (1991).
 - [4] M. Yoshida, K. Shiraki, S. Okubo, H. Ohta, T. Ito, H. Takagi, M. Kaburagi, and Y. Ajiro, Phys. Rev. Lett. **95**, 117202 (2005).
 - [5] F. Tedoldi, R. Santachiara, and M. Horvatić, Phys. Rev. Lett. **83**, 412 (1999).
 - [6] J. Das, A. V. Mahajan, J. Bobroff, H. Alloul, F. Alet, and E. S. Sørensen, Phys. Rev. B **69**, 144404 (2004).
 - [7] M. Takigawa, N. Motoyama, H. Eisaki, and S. Uchida, Phys. Rev. B **55**, 14129 (1997).
 - [8] K. Kudo, T. Noji, Y. Koike, T. Nishizaki, and N. Kobayashi, J. Phys. Soc. Jpn. **73**, 3497 (2004).
 - [9] S. El Shawish and J. Bonča, Phys. Rev. B **74**, 174420

- (2006).
- [10] S. Haravifard, S. R. Dunsiger, S. El Shawish, B. D. Gaulin, H. A. Dabkowska, M. T. F. Telling, T. G. Perring, and J. Bonča, *Phys. Rev. Lett.* **97**, 247206 (2006).
- [11] S. Capponi, D. Poilblanc, and F. Mila, *Phys. Rev. B* **80**, 094407 (2009).
- [12] B. S. Shastry and B. Sutherland, *Physica B+C* **108**, 1069 (1981).
- [13] H. Kageyama, K. Yoshimura, R. Stern, N. V. Mushnikov, K. Onizuka, M. Kato, K. Kosuge, C. P. Slichter, T. Goto, and Y. Ueda, *Phys. Rev. Lett.* **82**, 3168 (1999).
- [14] K. Kodama, J. Yamazaki, M. Takigawa, H. Kageyama, K. Onizuka, and Y. Ueda, *J. Phys.: Condens. Matter* **14**, L319 (2002).
- [15] S. Miyahara and K. Ueda, *Phys. Rev. Lett.* **82**, 3701 (1999).
- [16] A. Koga and N. Kawakami, *Phys. Rev. Lett.* **84**, 4461 (2000).
- [17] P. Corboz and F. Mila, *Phys. Rev. B* **87**, 115144 (2013).
- [18] K. Onizuka, H. Kageyama, Y. Narumi, K. Kindo, Y. Ueda, and T. Goto, *J. Phys. Soc. Jpn.* **69**, 1016 (2000).
- [19] K. Kodama, M. Takigawa, M. Horvatić, C. Berthier, H. Kageyama, Y. Ueda, S. Miyahara, F. Becca, and F. Mila, *Science* **298**, 395 (2002).
- [20] S. E. Sebastian, N. Harrison, P. Sengupta, C. D. Batista, S. Francoual, E. Palm, T. Murphy, N. Marcano, H. A. Dabkowska, and B. D. Gaulin, *Proc. Natl. Acad. Sci. USA* **105**, 20157 (2008).
- [21] M. Jaime, R. Daou, S. A. Crooker, F. Weickert, A. Uchida, A. E. Feiguin, C. D. Batista, H. A. Dabkowska, and B. D. Gaulin, *Proc. Natl. Acad. Sci.* **109**, 12404 (2012).
- [22] M. Takigawa, M. Horvatić, T. Waki, S. Kramer, C. Berthier, F. Levy-Bertrand, I. Sheikin, H. Kageyama, Y. Ueda, and F. Mila, *Phys. Rev. Lett.* **110**, 067210 (2013).
- [23] Y. H. Matsuda, N. Abe, S. Takeyama, H. Kageyama, P. Corboz, A. Honecker, S. R. Manmana, G. R. Foltin, K. P. Schmidt, and F. Mila, *Phys. Rev. Lett.* **111**, 137204 (2013).
- [24] For an early review, see S. Miyahara and K. Ueda, *J. Phys.: Condens. Matter* **15**, R327 (2003).
- [25] For a recent review, see M. Takigawa and F. Mila, *Introduction to Frustrated Magnetism*, edited by C. Lacroix, P. Mendels, and F. Mila (Springer, New York, 2011), p. 241.
- [26] H. Kageyama, K. Onizuka, T. Yamauchi and Y. Ueda, *J. Cryst. Growth* **206**, 65 (1999).
- [27] K. Kudo, T. Noji, Y. Koike, T. Nishizaki and N. Kobayashi, *J. Phys. Soc. Jpn.* **70**, 1448 (2001).
- [28] See the supplemental material at *****, which includes Refs. [26, 29–31], for details about the experiments and the theory.
- [29] A. Abragam, “*The principles of Nuclear Magnetism*” (Oxford Univ. Press, 1961).
- [30] M. Takigawa and G. Saito, *J. Phys. Soc. Jpn.* **55**, 1233 (1986).
- [31] C. H. Recchia, K. Gorny, and C. H. Pennington, *Phys. Rev. B* **54**, 4207 (1996).
- [32] A. Läuchli, S. Wessel, and M. Sigrist, *Phys. Rev. B* **66**, 014401 (2002).
- [33] R.D. Shannon, *Acta Cryst. A* **32**, 751 (1976).
- [34] M. E. Zayed, PhD thesis (EPFL, 2010); M.E. Zayed, Ch. Rüegg, E. Pomjakushina, M. Stingaciu, K. Conder, M. Hanfland, M. Merlini, H.M. Ronnow, *Solid State Comm.*

186, 13 (2014).

SUPPLEMENTAL MATERIALS

A. Magnetization due to impurity-induced free spins

Figure 5(a) shows the temperature dependence of the magnetization M of $\text{SrCu}_{2-x}\text{Zn}_x(\text{BO}_3)_2$ at the field of 1 T. The increase of M for $x = 0.0174$ and 0.0032 at low temperatures should be ascribed to the impurity-induced unpaired spins. By subtracting the magnetization for $x = 0$ from these data and normalizing by x , we obtain the contributions from the impurity-induced spins M_I , which are plotted in Fig. 5(a). The values of M_I are nearly identical for $x = 0.0174$ and 0.0032 in the whole temperature range, indicating that Zn^{2+} ions effectively replace the Cu sites. The increase of M_I below 10 K is described reasonably well by a free spin model $M_F = gS\mu_B B_S(X)$ with $S = 1/2$, where $B_S(X)$ ($X = gS\mu_B B/k_B T$) is the Brillouin function. Above 10 K, on the other hand, M_I is much smaller than M_F , indicating that Zn impurities can no longer generate free spins because of interaction between unpaired Cu spins and thermally excited triplets.

Figure 5(b) shows the magnetic field dependence of M at 2 K. Although the magnetization of a free spin M_F saturates completely above 4 T as indicated by the solid line, M of $\text{SrCu}_{2-x}\text{Zn}_x(\text{BO}_3)_2$ keeps increasing almost linearly with B at high fields. The NMR spectra shown in Fig. 6(a), on the other hand, indicate that the internal fields at boron sites stay exactly the same between 4.5 and 6.615 T, a clear indication of the saturation of the spin moments. The temperature dependence of the resonance frequency shown in Fig. 6(b) provides further support for the saturation of spin moments. Thus the linear increase of M at high fields cannot be attributed to spin moments. It may be associated with orbital (van Vleck) magnetism, even though we do not understand the mechanism for such a behavior. By subtracting the B -linear component at high fields from M , we obtain the contributions of the unpaired spins M_I , which are normalized by x and are plotted in Fig. 5(b). There is almost no difference between M_I for $x = 0.0174$ and 0.0032 . They also agree reasonably well with the free spin behavior M_F .

B. Dynamics of the impurity induced spins near saturation

When the impurity-induced moments become saturated as the temperature is decreased, we expect the thermal fluctuations to be gradually depressed and to slow down. Such a process has been indeed confirmed by measurements of the nuclear spin-lattice relaxation rate $1/T_1$ and of the spin-echo decay rate $1/T_2$. A standard inversion recovery method was used for the $1/T_1$ measure-

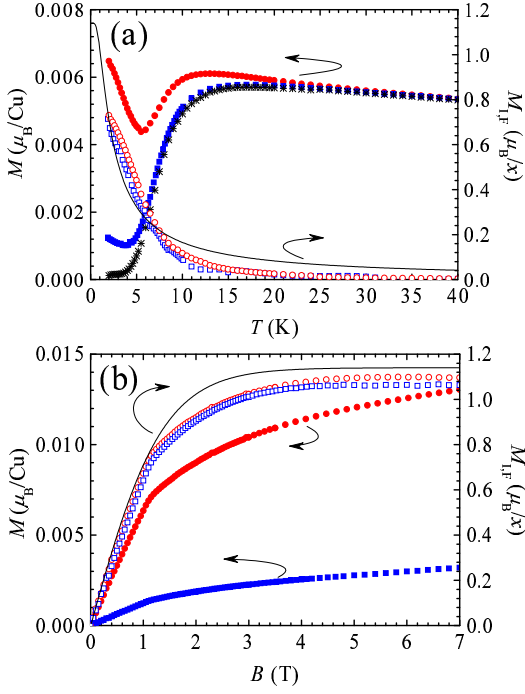


FIG. 5: (a) Temperature dependences of M at 1 T. (b) Magnetic field dependences of M at 2.0 K. The red solid circles, blue solid squares, and asterisks indicate M for $x = 0.0174$, 0.0032, and 0, respectively. The data of M for $x = 0$ is obtained from Ref. [26]. The red open circles and blue open squares indicate the contribution M_I from impurity-induced spins for $x = 0.0174$ and 0.0032, respectively. The solid line indicates the magnetization of a free spin M_F .

ment. To determine $1/T_2$, the spin echo intensity $I(\tau)$ as a function of the time τ between the two rf-pulses was fit to the exponential function $I(\tau) = C_0 \exp(-2\tau/T_2)$.

Figure 7 shows the temperature dependences of $1/T_1$ and $1/T_2$ measured on the low frequency quadrupole satellite line of the B_1 site at 6.615 T. Both $1/T_1$ and $1/T_2$ exhibit a peak but at different temperatures. The peak in $1/T_1$ occurs at 3.8 K while the peak in $1/T_2$ appears near 2.5 K. In fact, T_2 becomes too short near 2.5 K to be able to observe NMR signal. At lower temperatures, both $1/T_1$ and $1/T_2$ show steep decrease, consistent with the excitation gap for impurity induced spins in a magnetic field.

Let us first discuss $1/T_1$, which is related to the time correlation function of the local field by the standard formula, $1/T_1 \propto G(\omega_N)$, where $G(\omega) = \int \langle h(0)h(t) \rangle \exp(i\omega t) dt$ and ω_N is the NMR frequency. A simple expression for the correlation function parametrized by the mean square amplitude of the fluctuation $\langle h^2 \rangle$ and the correlation time τ_c , $\langle h(0)h(t) \rangle = \langle h^2 \rangle \exp(-t/\tau_c)$ leads to the following simple result,

$$1/T_1 \propto \langle h^2 \rangle \frac{\tau_c}{1 + (\omega_N \tau_c)^2}. \quad (3)$$

The saturation of the impurity-induced moments is ex-

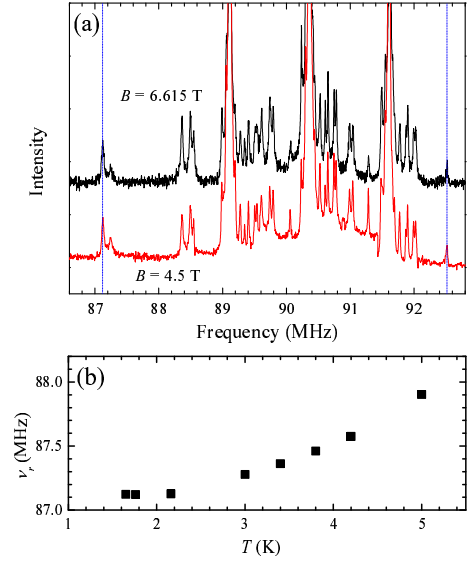


FIG. 6: (a) ^{11}B NMR spectra of $\text{SrCu}_{2-x}\text{Zn}_x(\text{BO}_3)_2$ with $x = 0.0174$ at 1.6 K for two different field values. The frequency for the spectrum at 4.5 T is shifted by 28.87 MHz to account for the difference in the nuclear Zeeman frequency. The position of the lines then match perfectly, indicating that the distribution of the spin moments remains the same for the two field values, hence that the impurity induced moments are saturated. (b) Temperature dependence of the peak frequency of the low frequency quadrupole satellite line of B_1 sites obtained at 6.615 T. It remains constant below 2.2 K, again indicating saturation of the impurity-induced moments.

pected to proceed with the depression of $\langle h^2 \rangle$ and the growth of τ_c . The peak in $1/T_1$ can be reproduced only by the latter process. Indeed $1/T_1$ exhibits a peak when $\tau_c = 1/\omega_N \sim 1.8 \times 10^{-9}$ s, a well known result in the context of motional narrowing in classical NMR [29].

The slowing down of the spin fluctuation can also cause a peak in $1/T_2$, with different criteria however. When the fluctuating local field slows down, the fastest spin-echo decay is achieved when $1/\tau_c$ becomes comparable to $\gamma\sqrt{\langle h^2 \rangle}$ and the peak value of $1/T_2$ has the same orders of magnitude as $1/\tau_c$ at the peak temperature [30, 31].

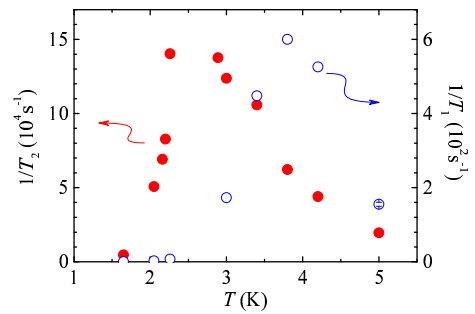


FIG. 7: Temperature dependence of $1/T_1$ (blue open circles) and $1/T_2$ (red solid circles) measured on the low frequency quadrupole satellite line of the B_1 site at 6.615 T.

Although we were not able to determine the peak value of $1/T_2$ due to loss of NMR signal, it should be of the order of 10^6 s^{-1} , judging from the data in Fig. 7, indicating that $\tau_c \sim 10^{-6} \text{ s}$ at 2.5 K, which is much longer than the value estimated at the peak temperature of $1/T_1$ (3.8 K). Thus, different peak temperatures of $1/T_1$ and $1/T_2$ provide evidence for a rapid but gradual slowing down of the fluctuation of the impurity-induced spins, which precedes the complete saturation at lower temperatures.

C. Comparison of the NMR spectra for different Zn concentration

Figure 8 shows the ^{11}B NMR spectra for $x = 0.0032$ and 0.0174 at 1.6 K and 6.615 T. Both samples show nearly identical spectra. All the resolved peaks are exactly at the same frequencies, indicating that the average distance between Zn^{2+} ions is sufficiently large and effects of interaction between impurity-induced spins can be neglected. However, the widths of the individual lines for $x = 0.0174$ are slightly larger than those for $x = 0.0032$, which is likely due to the difference in the distribution of the demagnetizing fields inside the crystals.

D. Numerical Methods

Exact Diagonalization (ED) have been performed using the standard Lanczos algorithm for the $S = 1/2$ Heisenberg model on Shastry-Sutherland lattices ($N = 32$ and 36 sites, see Fig. 9) having a single impurity. Periodic boundary conditions have been used to minimize finite-size effects. The presence of an impurity forbids to use any translation symmetry, but we have still made use of the remaining reflection symmetry to reduce the size of the Hilbert space. After computing the ground-state, one can easily extract the average magnetization on each site. Note that since the polaron has a large but finite extension beyond which the magnetization becomes very small, one can expect a priori the finite-size

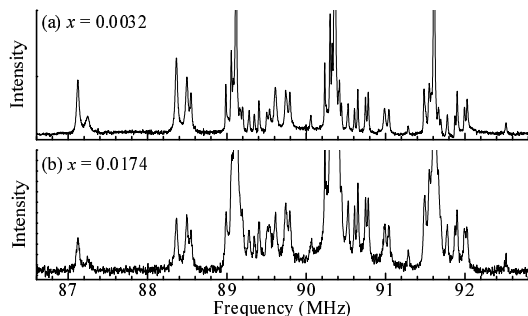


FIG. 8: ^{11}B NMR spectra of $\text{SrCu}_{2-x}\text{Zn}_x(\text{BO}_3)_2$ with $x = 0.0032$ (a) and 0.0174 (b) at 1.6 K and 6.615 T.

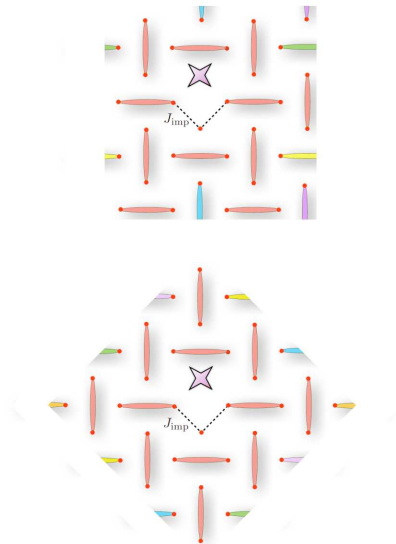


FIG. 9: Clusters used for the simulations with 32 sites (top) and 36 sites (bottom) and one impurity represented as a cross. Colored dimers correspond to strong J bonds while J' bonds are not shown for clarity (except the J_{imp} bonds introduced in the main text). Periodic boundary conditions are used to minimize finite-size effects, so that colored dimers crossing the boundaries can be easily identified with different colors.

effects to be small. This is confirmed by a comparison of the results obtained on 32-site and 36-site clusters, for which the magnetizations are nearly identical, a conclusion further confirmed by calculations on larger clusters up to 64 sites with infinite Product Entangled Pair State simulations [P. Corboz, private communication]. We are thus confident that the local magnetizations reported in this work are close to their thermodynamical values (see Fig. 3c of the main text).

E. Intensity and line shape of some specific lines.

One of our main conclusion that $\langle S_c^A \rangle < \langle S_c^C \rangle$ is based on the intensity ratio of the B_1 and B_2 lines, which are assigned to the B sites close to Cu_C and Cu_A on the layer of the Zn impurity. Equally important is the intensity ratio of the B_{11} and B_{12} lines assigned to the B sites on the adjacent layers coupled to Cu_C and Cu_A with the same dipolar coupling D_3 . The spectrum of the center line of these sites are displayed in Fig. 10(a) with an enlarged scale. We can clearly see that the integrated intensity of the B_{12} line is twice as large as the B_{11} line. Since Cu_C is twice as abundant as Cu_A , the B_{12} (B_{11}) line must be assigned to the neighbor of Cu_C (Cu_A). The fact that B_{int} is larger for the B_{12} line than for the B_{11} line then leads to the conclusion that $\langle S_c^A \rangle < \langle S_c^C \rangle$.

The ED calculation shows that there is another pair of lines (10 and $10'$) assigned to the B sites on the adjacent layers coupled to Cu_C and Cu_A with the smaller

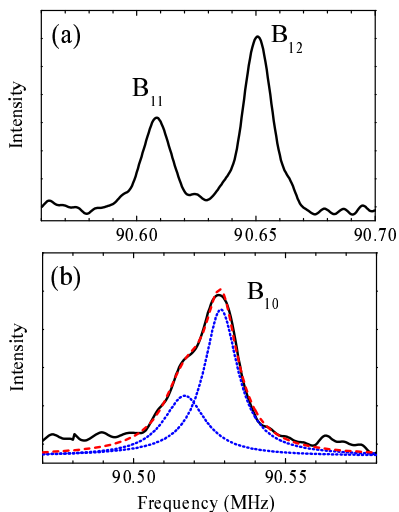


FIG. 10: Enlarged NMR spectra for the center lines of (a) B_{11} and B_{12} and (b) B_{10} lines..

dipolar coupling D_4 (see the upper panel of Fig. 4b of the main text). Although the experimentally observed B_{10} line shows only a single peak, the spectral shape can be actually fit well to a sum of two Lorentzians with the intensity ratio of 2 to 1 as indicated in Fig. 10(b). The fact that one of these lines with larger B_{int} has the double intensity is again consistent with the conclusion $\langle S_c^A \rangle < \langle S_c^C \rangle$.

There is a puzzle though. Since the two pairs of lines are coupled to the same pair of Cu sites (Cu_C and Cu_A) with different dipolar couplings, their separation should be equal to the ratio of the dipolar couplings $D_3/D_4 = 1.58$. However, this ratio in the experimental spectrum is much larger (nearly 3). This suggests that the internal fields at the B sites in the adjacent layers are not entirely due to the in-plane Cu moments and that small contributions from induced moments on Cu sites in the adjacent layers due to interlayer exchange may be relevant. To explore such effects is beyond the scope of this paper however.

For other experimental lines $B_6 - B_9$, the resolution is not sufficient to achieve a one to one correspondence with the calculated lines. However, the assignment of lines B_8 and B_9 to the pairs of theoretical lines (8, 8') and (9, 9') is plausible since they are well separated from the others. Finally, the lines B_6 and B_7 develop on top of the broad tail of the main line, consistent with the numerous theoretical lines on the negative side of the main line, even though specific assignment is not possible.

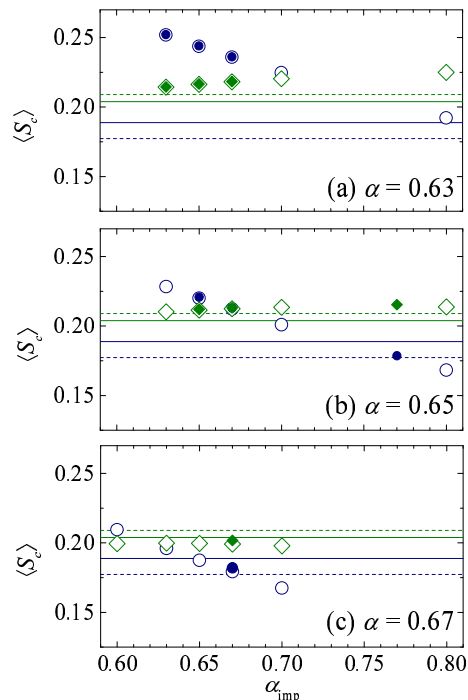


FIG. 11: Local magnetization at Cu_A ($\langle S_c^A \rangle$, circles) and Cu_C ($\langle S_c^C \rangle$, squares) calculated by exact diagonalization for a cluster with 32 (open symbols) or 36 (filled symbols) sites are plotted against $\alpha_{\text{imp}} = J_{\text{imp}}/J$ for three values of bulk $\alpha = J'/J$. The horizontal lines indicate the values of $\langle S_c^A \rangle$ and $\langle S_c^C \rangle$ determined from the values of B_{int} at the B sites on the same layers as the Zn impurity (the solid lines) or on the neighboring layers (the dashed lines).

F. Possible local change of exchange interaction due to lattice distortion

Here we employ a simple model to account for a possible change of exchange interaction due to local lattice distortion near Zn impurities and examine to what extent our best choice of $\alpha = 0.665$ is influenced by such effects. Since the distribution of ν_Q shown in Fig. 3(b) of the main text suggests that the lattice distortion is confined in the immediate vicinity of Zn, the simplest model consists in assuming that only the exchange interaction for the Cu-Cu bonds closest to the Zn impurity, i.e. the exchange between Cu_A and Cu_B , changes from the bulk J' to J_{imp} (see Fig. 9).

We have calculated the moments at Cu_A and Cu_C sites by exact diagonalization using a cluster of 32 or 36 sites as a function of $\alpha_{\text{imp}} = J_{\text{imp}}/J$ for three values of the bulk ratio $\alpha = J'/J'$, 0.63, 0.65, and 0.67. The results plotted in Fig. 11 indicate that $\langle S_c^A \rangle$ decreases rapidly with α_{imp} . However, $\langle S_c^C \rangle$ stays nearly constant or even increases slightly with α_{imp} . Therefore, the condition $\langle S_c^A \rangle < \langle S_c^C \rangle$ can be met for α smaller than 0.66 if we allow for a large value of α_{imp} as demonstrated in Fig. 11.

To make a quantitative comparison with the experi-

mental data, we extracted the local magnetization from the observed values of B_{int} . First, we used the values of B_{int} at seven B sites on the layer of the impurity (B_{1-4} and B_{13-15} in Fig. 4b of the main text), each of which is the nearest neighbor to one of the major Cu sites ($\text{Cu}_{\text{A-G}}$) carrying appreciable moments. The values of $\langle S_c^{\text{A-G}} \rangle$ can be determined by solving Eq. (2) after substituting the experimental values of B_{int} into the left side and using the same values of the hyperfine coupling constants $T_1 = -0.563$ T. The values of Cu_{A} and Cu_{C} thus determined are shown by the solid lines in Fig. 11. Alternatively, we can use the values of B_{int} at the B sites

in the adjacent layers (B_5 , B_{11} , and B_{12}) coupled to the three major Cu sites ($\text{Cu}_{\text{A-C}}$) by the dipolar coupling D_3 to determine $\langle S_c^{\text{A-C}} \rangle$. The results are displayed by the dashed lines in Fig. 11. From these plots, we may conclude that the experimental results can be reconciled with $\alpha = 0.65$ by allowing a rather large modification of exchange coupling near Zn. The value $\alpha = 0.63$ seems difficult to reconcile with the experimental results within this simple model, but these results make it plausible that allowing for additional modifications slightly further away from Zn can further reduce the value of α .